Title
Subdiffusive transport of fluctuating elastic filaments in cellular flows

Journal
Physics of Fluids, 25(7)

ISSN
1070-6631

Authors
Manikantan, Harishankar
Saintillan, David

Publication Date
2013-07-01

DOI
10.1063/1.4812794

Peer reviewed

PHYSICS OF FLUIDS **25**, 073603 (2013)

Subdiffusive transport of fluctuating elastic filaments in cellular flows

Harishankar Manikantan and David Saintillan[a)]
Department of Mechanical Science and Engineering, University of Illinois at Urbana-Champaign, Urbana, Illinois 61801, USA

(Received 2 April 2013; accepted 19 June 2013; published online 10 July 2013)

The dynamics and transport properties of Brownian semiflexible filaments suspended in a two-dimensional array of counter-rotating Taylor-Green vortices are investigated using numerical simulations based on slender-body theory for low-Reynolds-number hydrodynamics. Such a flow setup has been previously proposed to capture some of the dynamics of biological polymers in motility assays. A buckling instability permits elastic filaments to migrate across such a cellular lattice in a "Brownian-like" manner even in the athermal limit. However, thermal fluctuations alter these dynamics qualitatively by driving polymers across streamlines, leading to their frequent trapping within vortical cells. As a result, thermal fluctuations, characterized here by the persistence length, are shown to lead to subdiffusive transport at long times, and this qualitative shift in behavior is substantiated by the slow decay of waiting-time distributions as a consequence of trapping events during which the filaments remain in a particular cell for extended periods of time. Velocity and mass distributions of polymers reveal statistically preferred positions within a unit cell that further corroborate this systematic shift from transport to trapping with increasing fluctuations. Comparisons to results from a continuum model for the complementary case of rigid Brownian rods in such a flow also highlight the role of elastic flexibility in dictating the nature of polymer transport.
[http://dx.doi.org/10.1063/1.4812794]

I. INTRODUCTION

Semiflexible elastic filaments, such as DNA, actin, and microtubules, play a central role in a wide variety of biological processes from locomotion[1] to reproduction[2] to cell division.[3] The analysis of their dynamics and transport properties in microscale fluid flows is therefore of paramount importance for the understanding and accurate modeling of these processes. The case of long-chain polymers such as DNA has been studied in detail in the past,[4,5] and both experiments and numerical simulations have established that the dynamics of such chains are governed by the competition of entropic forces that favor coiled configurations vs viscous flow forces that can cause unraveling and stretching.[4,6–8] This competition is at the origin of the viscoelastic properties of DNA solutions,[4,9] which can lead to hydrodynamic instabilities[10,11] and spatiotemporally chaotic flows.[12] The case of shorter and stiffer filaments with long persistence lengths, such as actin and microtubules, has received much less attention and is of interest to us here. For short-chain semiflexible filaments, the dynamics result mainly from the interplay between internal elastic forces that resist bending and ensure inextensibility, and external viscous forces that can cause deformations and buckling.

Much like a macroscopic beam, an elastic filament under compression along its backbone can undergo a buckling instability if compressive stresses overcome the elastic restoring force that resists bending. Such buckling events were first noted by Becker and Shelley[13] in simulations of non-Brownian flexible fibers in simple shear flow at high enough strain rate, and the storage and

a)Electronic mail: dstn@illinois.edu

subsequent release of elastic energy during this process has been shown to lead to first normal stress differences,[13,14] as are indeed known to arise in many polymer solutions.[9]

These buckling events are more easily analyzed in irrotational linear flows such as planar extensional flows, where a filament located at the hyperbolic stagnation point and aligned with the axis of compression of the flow is subject to a compressive tensile force. Using linearized Euler-Bernoulli elasticity and slender-body theory[15] for Stokes flow, Young and Shelley[16] showed that this situation is amenable to a linear stability analysis and found that beyond a critical strain rate a non-Brownian elastic filament undergoes a compressive buckling instability analogous to Euler buckling in beams, and this instability has come to be known as the *stretch-coil transition*.[16] As the strain rate (and hence the tension in the filament) increases, higher mode shapes can become unstable and corresponding thresholds for each successive filament shape have been calculated.[16] This buckling instability appears to be a generic feature of strain-dominated flows when the polymer is aligned along a direction of compression, and the case of an elastic filament tethered normal to a rigid wall at the stagnation point of a compressive extensional flow was also recently discussed by Guglielmini *et al.*[17]

The results of the stability analysis of Young and Shelley,[16] though strictly valid in the absence of thermal fluctuations, were also recently tested experimentally by Kantsler and Goldstein[18] using actin filaments trapped at the stagnation point of a microfluidic cross-slot device, where buckling was indeed observed. A succession of mode shapes was also reported with increasing strain rate. The instability, however, no longer occurred at a critical flow strength but was seen to gradually transition from the straight (though susceptible to thermal fluctuations) state to the buckled state in the vicinity of the theoretical athermal threshold. To quantify the extent of buckling, Kantsler and Goldstein tracked the mean end-to-end distance as a function of the imposed strain rate. As opposed to the sharp cusp expected at the instability threshold in the non-Brownian limit, they found that thermal fluctuations strongly round the transition, as is already known to be the case for classic Euler buckling.[19]

Such buckling events can be a significant driving factor behind transport properties of elastic filaments. One example of this effect comes from actin motility assays,[20–22] in which actin filaments are transported over a two-dimensional carpet of wall-tethered myosin molecular motors. These assays are typically characterized by motility defects, wherein a polymer gets pinned at its leading tip causing it to buckle in plane and curl up towards the tip.[20,21] The pinned tip eventually breaks free, allowing the filament to continue to move in a different direction. In cases of high myosin density, the result of these dynamics is a meandering motion with every instance of buckling randomly changing the direction the polymer is headed. The prevalence of polymer buckling in complex flows of elastic filaments has also been reported in other biophysical systems, such as two-dimensional suspensions of microtubule bundles and kinesin clusters,[23] where stretching of the bundles as a result of the relative sliding of individual microtubules under the action of the kinesin motors can cause them to deform and buckle.

A simple illustration of the relation between buckling and spatial transport was also provided by Young and Shelley,[16] who proposed that a periodic lattice of steady counter-rotating Taylor-Green vortices in a viscous incompressible fluid can capture some of the dynamics observed in actin motility assays. The vortices create hyperbolic junctions connected by straight streamlines, defining "cells" that enclose an entire family of closed curved streamlines as illustrated in Fig. 1. An initially straight filament placed along one of the edges is transported along the straight streamline until it approaches a stagnation point. There, the flow is locally an extensional flow, and the aforementioned linear stability analysis predicts a buckling event if the local strain rate is sufficiently high. The "stretched" filament is expected to slow down and buckle or "coil" (analogous to pinning and curling in actin motility assays), and to subsequently relax to a stretched configuration in an arbitrarily chosen perpendicular direction. Using non-Brownian simulations, Young and Shelley[16] indeed showed that an elastic filament in such a flow moves across the lattice like a random walker executing arbitrary $\pi/2$ turns at each hyperbolic junction. On long time scales, such a random walk was found to be diffusive in the absence of thermal fluctuations, at least over a certain range of flow strengths. Recent experiments by Wandersman *et al.*[24] and by Quennouz[25] using macroscopic elastic fibers in an electrodynamically generated cellular flow similar to that used by Young and Shelley[16] indeed

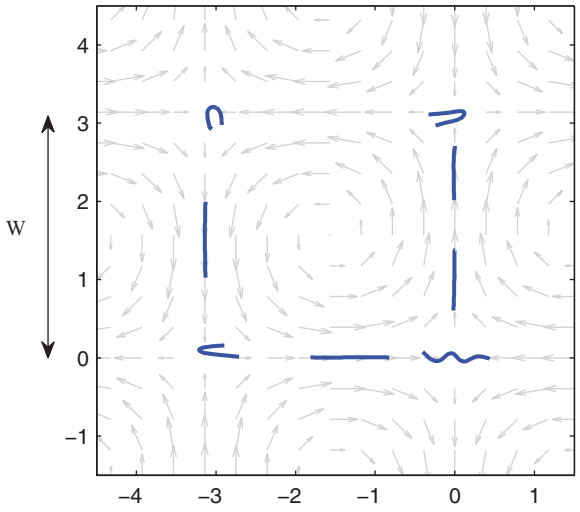

FIG. 1. Snapshots from a simulation with $\bar{\mu} = 80\,000$, $\ell_p/L = 1000$, and $w = 1$, showing the buckling instability at the stagnation points at cell corners.

verified predictions from their simulations and clearly showed the relevance of the stretch-coil transition on the dynamics. By tuning the flow strength and mechanical properties of the fibers, they[24,25] measured the onset and probability of buckling in terms of an elastoviscous number S_p and observed good agreement with the predictions of the stability analysis[16] within experimental limitations. They confirmed that flexibility facilitates transport between and across cells as a result of buckling, and observed random trajectories akin to those obtained by Young and Shelley,[16] albeit on shorter scales owing to the limited size of the flow device used in the experiments.

A central question that has yet to be addressed and is directly relevant to the transport of biological polymers such as actin is the effect of thermal fluctuations on the dynamics, and this work is the first comprehensive attempt at addressing this issue. Using numerical simulations based on a slender-body model with a stochastic Brownian force distribution obeying the fluctuation-dissipation theorem, we systematically analyze the effect of Brownian fluctuations (measured by the persistence length of the polymer) on the dynamics of isolated chains in a periodic Taylor-Green vortex flow. Our main finding is that in the limit of infinite dilution, fluctuations have a tendency to cause the more frequent trapping of the filaments inside cells, thereby hindering their ability to diffuse in the plane of the flow; in fact, we even observe a transition to subdiffusive transport as the persistence length is decreased. Details of the polymer model and simulation method are provided in Sec. II. We discuss results in Sec. III, where we analyze the effect of fluctuations on transport properties, velocity distributions, and mass distributions of the filaments, and also compare our results to the case of rigid Brownian fibers. We conclude in Sec. IV.

II. POLYMER MODEL

A. Slender-body equations

Slender-body theory for low-Reynolds-number hydrodynamics dates back to Batchelor,[15] and was developed by asymptotically matching the near-field flow around a slender particle represented as an infinitely long cylinder to the far-field flow driven by a line distribution of force singularities along the particle axis. In this work, we consider a local version of the theory[14,16] that accounts for anisotropy of drag due to the shape of the filament, but does not capture hydrodynamic interactions within a polymer or between polymer chains.

Let a filament of length L be parameterized by an arclength $s \in [0, L]$ such that $\mathbf{x}(s) = (x(s), y(s), z(s))$ represents the polymer centerline. We define a slenderness ratio $\epsilon = r(L/2)/L$ where the polymer is assumed to have a circular cross-section with radius $r(s)$. Then, the local

slender-body equation for the dynamics of the filament centerline is written as

$$8\pi\mu\left(\frac{\partial \mathbf{x}(s,t)}{\partial t} - \mathbf{u}_0(\mathbf{x}(s,t),t)\right) = -\mathbf{\Lambda}(s)\cdot\mathbf{f}(s). \tag{1}$$

Here, μ denotes the fluid viscosity, $\mathbf{u}_0(\mathbf{x}(s,t),t)$ is the background fluid velocity felt by the polymer at $\mathbf{x}(s,t)$, $\mathbf{\Lambda}(s)$ is the local mobility operator, and $\mathbf{f}(s)$ is the net force acting *on* the filament at parametric position s. The mobility operator is given by

$$\mathbf{\Lambda}(s) = -\ln(\epsilon^2 \mathrm{e})(\mathbf{I} + \hat{\mathbf{p}}(s)\hat{\mathbf{p}}(s)) + 2(\mathbf{I} - \hat{\mathbf{p}}(s)\hat{\mathbf{p}}(s)), \tag{2}$$

where $\hat{\mathbf{p}}(s) = \mathbf{x}_s(s)$ is the local unit tangent vector to the polymer backbone, and $\hat{\mathbf{p}}\hat{\mathbf{p}}$ denotes a dyadic product.

The forces acting on the filament are threefold: bending forces due to the elasticity of the polymer backbone, line tension that acts to keep it inextensible, and Brownian forces due to thermal fluctuations in the medium:

$$\mathbf{f}(s) = -(\sigma\mathbf{x}_s)_s + \kappa\mathbf{x}_{ssss} + \mathbf{f}^{br}, \tag{3}$$

where subscripts denote differentiation with respect to the concerned variable. The first two terms follow directly from Euler-Bernoulli elasticity, with $\sigma(s)$ being the non-uniform tension felt by the filament, and κ being the bending modulus. The last term obeys the fluctuation-dissipation theorem[26] of statistical mechanics:

$$\left\langle \mathbf{f}^{br}(s,t)\right\rangle = \mathbf{0}, \tag{4a}$$

$$\left\langle \mathbf{f}^{br}(s,t)\mathbf{f}^{br}(s',t')\right\rangle = 2k_B T\mathbf{\Lambda}^{-1}\delta(s-s')\delta(t-t'), \tag{4b}$$

where k_B is Boltzmann's constant and T is the absolute temperature. Note that the line tension $\sigma(s)$, which acts as a Lagrange multiplier to keep the filament inextensible, is still unknown at this point. It is obtained by imposing a local inextensibility condition, i.e., by enforcing that the unit tangent vector maintains magnitude. Assuming that the arclength parameter s is a material property, this permits us to perform the following manipulation:

$$\mathbf{x}_s\cdot\mathbf{x}_s = 1 \Rightarrow (\mathbf{x}_s\cdot\mathbf{x}_s)_t = 0 \Rightarrow \mathbf{x}_s\cdot\mathbf{x}_{ts} = 0. \tag{5}$$

Equation (1) can be used for $\mathbf{x}_t$ here, leading to an inhomogeneous ordinary differential equation for $\sigma(s)$ that is coupled to the centerline equation,[14] and the two can be solved together to obtain the line tension and the position $\mathbf{x}(s,t)$ of the polymer backbone. The ends of the polymer are "free," i.e., there are no forces or moments acting at the ends. This transcends into the boundary conditions:[14,18,26]

$$\mathbf{x}_{ss}|_{s=0,L} = \mathbf{x}_{sss}|_{s=0,L} = \sigma|_{s=0,L} = 0. \tag{6}$$

B. Non-dimensionalization

All lengths are made dimensionless by L, deterministic forces by κ/L^2, and time by $8\pi\mu L^4/\kappa$. Following Munk *et al.*,[26] Brownian forces are scaled by $\sqrt{(L/\ell_p)}\kappa/L^2$, where the persistence length ℓ_p is defined below; this allows the dimensionless Brownian force distribution to be a function only of the mobility operator. The external flow field is made dimensionless by $L\dot{\gamma}$, where $\dot{\gamma}$ is the characteristic flow strength associated with the background fluid velocity. The centerline equation (1) then becomes

$$\frac{\partial \mathbf{x}(s,t)}{\partial t} = \bar{\mu}\mathbf{u}_0(\mathbf{x}(s,t),t) - \mathbf{\Lambda}\cdot\left[-(\sigma\mathbf{x}_s)_s + \mathbf{x}_{ssss} + \sqrt{\frac{L}{\ell_p}}\boldsymbol{\xi}\right], \tag{7}$$

where all variables are now dimensionless, and $\boldsymbol{\xi}$ denotes the dimensionless noise term. The tension equation obtained from Eq. (5) can also be made dimensionless after further manipulations using properties of the unit tangent vector.[14]

We have introduced two dimensionless groups that control the dynamics of the problem. The first is an *effective viscosity* $\bar{\mu}$, which is the ratio of the characteristic viscous drag to the elastic bending force in the polymer backbone:

$$\bar{\mu} = \frac{8\pi\mu L^2\dot{\gamma}}{\kappa/L^2}, \tag{8}$$

and can also be interpreted as a dimensionless flow strength. This parameter is equal to $32S_p$ and $4\pi^4 \ln(1/\epsilon^2 \mathrm{e})\Sigma$ in the notations of Wandersman *et al.*[24] and of Kantsler and Goldstein,[18] respectively.

The second dimensionless group is the *reduced persistence length*:

$$\frac{\ell_p}{L} = \frac{\kappa/L^2}{k_B T/L} = \frac{\kappa}{k_B T L}, \tag{9}$$

which can be interpreted as the ratio of the elastic bending forces to thermal forces. In other words, ℓ_p is the length scale over which these forces strike a balance and the local tangent vector becomes uncorrelated. A large value of ℓ_p hence implies large bending resistance to thermal fluctuations, while smaller values represent floppier polymer backbones. To put things in perspective, the persistence length of microtubules as calculated using Eq. (9) above is found[27] to be ∼5 mm, while that of actin filaments[18] is ∼18 μm. As the length of these biopolymers is of the order of a few micrometers, the reduced persistence length ℓ_p/L for microtubules and actin is of the order of $\mathcal{O}$(100–1000) and $\mathcal{O}$(1–10), respectively.

The dimensionless centerline equation (7) along with the equation for the tension are solved numerically using a Brownian dynamics algorithm extending the method previously developed by Tornberg and Shelley[14] for non-Brownian elastic filaments. The aspect ratio is chosen to be $\epsilon = 0.01$ for the entire work presented here. The algorithm has been tested to accurately predict equilibrium properties of worm-like chain polymers in Brownian solvents, and details will be presented elsewhere.

C. Cellular flow and the buckling instability

In this study, we consider the transport of a flexible Brownian filament in a prescribed flow field consisting of a two-dimensional periodic array of counter-rotating Taylor-Green vortices:

$$\mathbf{u}_0(\mathbf{x}) = (\sin(x/w)\cos(y/w), -\cos(x/w)\sin(y/w), 0), \tag{10}$$

where x and y are made dimensionless with L as usual, and $w = W/\pi L$ is the dimensionless cell size (see Fig. 1). Note that this imposed flow field is two-dimensional, while we will be allowing for three-dimensional motion of the polymer arising solely from thermal fluctuations, unlike in the previous simulations of Young and Shelley[16] and the experiments of Wandersman *et al.*,[24] where the filaments were confined on a two-dimensional interface.

As was described earlier, a polymer in the vicinity of one of the stagnation points in such a flow experiences a locally hyperbolic extensional flow. Within this approximation, the linear stability results for the buckling instability should hold, for which, in the language of this work, the first (and from here on, the "critical") threshold[16] is $\bar{\mu}_c \approx 1250$. It can be shown that increasingly higher buckling modes become unstable above subsequent thresholds ($\bar{\mu} \approx 6400,\ 16\,000,\ 30\,000, \ldots$). These thresholds, again, remain broadly consistent even in the presence of thermal fluctuations.[18]

III. RESULTS AND DISCUSSION

A. Polymer transport: Diffusion vs subdiffusion

In the following, we focus entirely on flow strengths that exceed the critical threshold ($\bar{\mu} > \bar{\mu}_c$). The objective is to systematically describe the change in transport properties of a polymer in a cellular flow due to thermal fluctuations, in a regime where buckling events at the hyperbolic points of the vortex array already lead to "Brownian-like" transport across the lattice.[16]

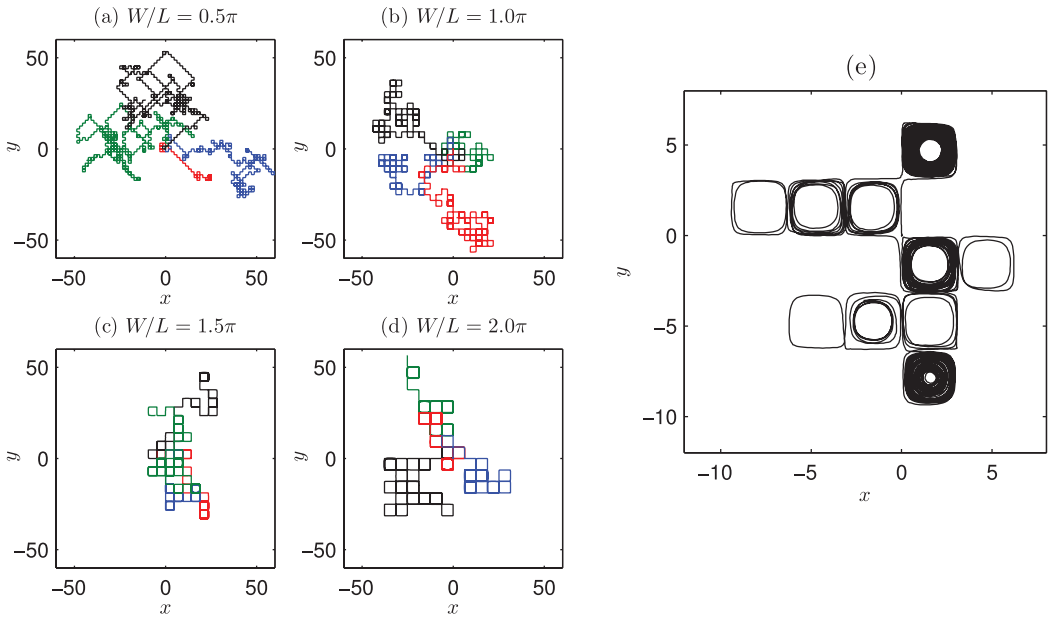

FIG. 2. Center-of-mass trajectories of polymers: (a)–(d) correspond to four different cell sizes W at the same $\bar{\mu} = 20\,000$ and $\ell_p/L = 1000$, each showing four different trajectories; (e) shows the case of a single polymer with $W = \pi L$ and $\bar{\mu} = 20\,000$, but $\ell_p/L = 10$ (enhanced online). [URL: http://dx.doi.org/10.1063/1.4812794.1]

The center-of-mass trajectories of a few representative cases are illustrated in Fig. 2 and the accompanying video. The key observation is that while a larger reduced persistence length allows polymers to migrate farther away from their initial position (the origin, in the case of the examples in Fig. 2), those with smaller reduced persistence lengths exhibit much slower transport from their initial position. Fig. 2(e) for the low value of $\ell_p/L = 10$ shows a characteristic trap-and-go motion wherein a polymer appears to be trapped in a cell for significantly longer time periods before escaping to another neighboring cell. This is qualitatively different from previous observations in non-Brownian experiments[24] and simulations,[16] which are comparable to the case of $\ell_p/L = 1000$. In this context, Young and Shelley[16] calculated a "transport region" enveloping the unit cell boundary that recorded a trapping probability of less than 50%. Their observation was that for a range of values of $\bar{\mu}$, filaments placed in this region would migrate across the lattice like a random walker and undergo a diffusive motion in space at long times as a result. Our simulations for $\ell_p/L = 1000$ show a similar behavior [Figs. 2(a)–2(d)], with relatively rare trapping occasions. This suggests that transport in this regime is akin to the non-Brownian case, with thermal fluctuations only changing the outcome from transport to trapping in very few cases. The dynamics are qualitatively different when $\ell_p/L = 10$, where we find that such a transport region cannot be defined. The effect of thermal fluctuations is very strong in this case, and as seen in Fig. 2(e) polymers often become trapped and migrate deep into a cell, only to jump out and transition to a neighboring cell at a later time and further proceed in this trap-and-go fashion. It should be noted here that for all our simulations, the polymer is released at the cell boundaries: we expect the probability of such trapping events to be significantly higher if the filament were released near the center of a cell.

It is interesting to compare the dynamics seen in Fig. 2 and in the accompanying video to that of a particle moving randomly across a periodic lattice with specified distributions of length and frequency of jumps.[28,29] Jumps of unit cell length at a fixed rate give rise to the traditional random walk, one that approaches the behavior predicted by a diffusion equation. If the jumps follow a heavy-tailed length distribution but still occur at a fixed rate, then it leads to so-called Lévy flights characterized by superdiffusion. The complementary case is that of "fractal time,"[28] which applies particularly to the behavior seen in Fig. 2(e), where a walker always moves a unit cell length but waits disparate amounts of times between jumps. For such random walks, the mean square displacement

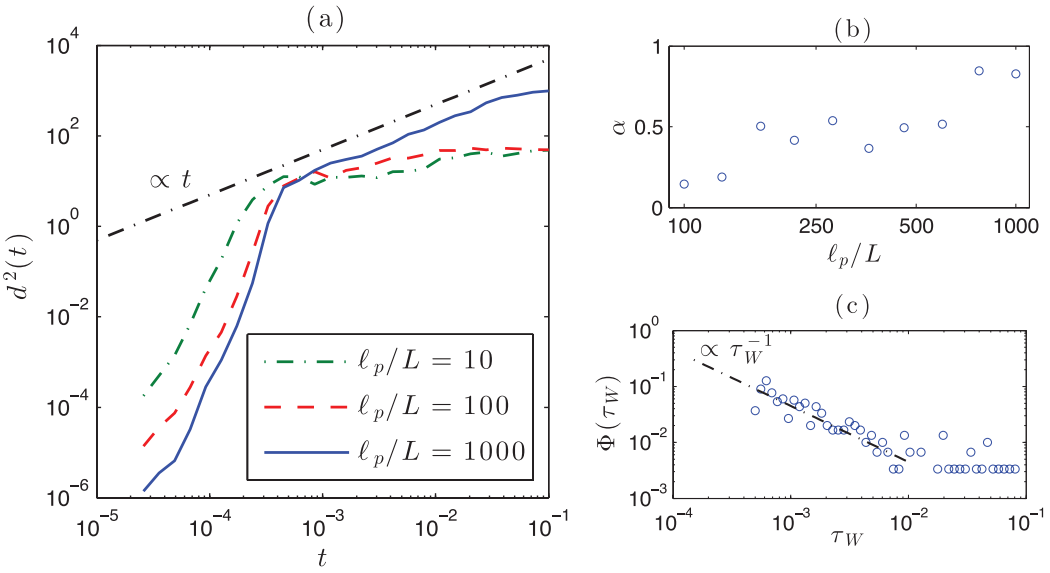

FIG. 3. (a) Mean square displacement $d^2(t)$ of the filament center-of-mass as a function of time at $\bar{\mu} = 20\,000$ for three values of ℓ_p/L, where the long-time behavior follows an approximate power law $d^2(t) \propto t^\alpha$. (b) Dependence of the exponent α on the reduced persistence length ℓ_p/L. (c) Distribution of waiting times, defined as periods of time spent by a filament inside a given cell, in simulations with $\bar{\mu} = 20\,000$ and $\ell_p/L = 10$.

is slower than that of a diffusive process, and numerical studies[29] have reported such waiting times leading to subdiffusion.

The diffusivity of polymers across the cellular lattice in the current problem can be characterized by the mean square displacement of the center of mass $\mathbf{x}_0(t)$ of a chain from its initial position: $d^2(t) = \langle |\mathbf{x}_0(t) - \mathbf{x}_0(0)|^2 \rangle$ (Fig. 3). Recall that we only consider isolated polymers, corresponding to the limit of an infinitely dilute suspension where the effects of the disturbance velocity due to other chains on the transport properties are negligible. These results are ensemble averages of 50 simulations for each value of ℓ_p/L shown, and were all obtained for $\bar{\mu}$ =20 000. The initial condition is the same but thermal fluctuations soon change the long-time dynamics in each simulation. For $\ell_p/L = 1000$, we observe a roughly linear increase in the mean square displacement with time, consistent with the case of non-Brownian filaments.[16] The initial climb in the beginning corresponds to the motion of the polymer moving along a cell boundary until it encounters the first stagnation point. For subsequent smaller values of $\ell_p/L = 100$ and 10, the initial climb is larger because the polymer no longer moves along the cell edges but rather is pushed further in towards the center of the cell by thermal fluctuations, thereby increasing the average distance traversed before it encounters the first stagnation point. Beyond this initial climb, however, the growth of the mean square displacement exhibits a clear subdiffusive behavior of the form $d^2(t) \propto t^\alpha$ with $\alpha < 1$. Within the timespan of the simulations, we observe that the slope of $d^2(t)$ in a log-log plot in fact reduces to almost zero in these cases. The filament tends to become trapped in almost every cell it comes by, and the occasional jump from cell to cell is seen in the very small positive slope in Fig. 3(a). In many cases, the filament even remained trapped in a given cell until the simulation had to be stopped. The precise dependence of the exponent α on the persistence length is shown in Fig. 3(b), where it is seen to transition from nearly zero for low values of ℓ_p/L to approximately 1 for high persistence lengths.

This transition from diffusive to subdiffusive transport with decreasing ℓ_p/L can be further characterized by considering the waiting-time distribution of the polymer in a cell, shown for $\ell_p/L = 10$ in Fig. 3(c). The waiting time τ_W is defined as the time a polymer spends within a given cell (quantified by its center-of-mass position). While moving along the boundary between cells, the center-of-mass often abruptly jumps back and forth between them. We discard these small values of τ_W by introducing a cutoff on the recorded waiting times: only those values of τ_W that are above the average time it takes a polymer to go on an entire loop around a cell are considered.

Also, we discard cases when the polymer gets trapped at the center of the cell and stays there for the entire span of the simulation. This distribution for the smaller values of the reduced persistence length displays approximately a power-law behavior that goes as $\Phi(\tau_W) \propto \tau_W^{-1}$. Such distributions of waiting times that follow a non-integrable form of $\Phi(\tau_W) \propto \tau_W^{-(1+\alpha)}$ with $\alpha < 1$ have been predicted theoretically[30] and reported in various physical systems[31,32] to result in subdiffusion with a mean square displacement growing as t^α. According to this prediction, the exponent α is expected to be nearly zero in the case of $\ell_p/L = 10$, which is indeed very close to what is observed for the slope of $d^2(t)$ in Fig. 3(a). This qualitative change in the waiting-time distribution clearly confirms that polymer trapping is indeed enhanced by thermal fluctuations.

B. Velocity distributions

In the actin motility experiments of Bourdieu *et al.*,[20,21] the frequency distribution of the velocity of the polymer was found to be bimodal at select temperatures. This bimodality was attributed to the "slip-stick" nature of polymer transport, in which periods of regular motion at a roughly constant velocity alternate with states when the polymer becomes pinned and the velocity is almost zero. In the present model, similar dynamics are expected in the case of $\ell_p/L = 1000$, when Brownian motion plays a negligible role in disturbing this cycle of motion-and-stagnation. This is indeed the case, as seen in Fig. 4(a) where we show the normalized frequency distribution of the center-of-mass velocity magnitude $|\mathbf{x}_t^0|$, which agrees qualitatively with the experiments[21] and quantitatively with non-Brownian simulations.[16] One noticeable difference is the presence of a minor peak near 0.7, which represents the rare occasions when the polymer does get trapped in a cell. The value of $|\mathbf{x}_t^0| = 0.7$ for the velocity in the trapped state is not very obvious, but one can see that it approximately corresponds to the largest ring of uniform velocity within a particular cell [Fig. 4(b)].

Thermal fluctuations change this picture drastically, as seen for lower values of the reduced persistence length. For $\ell_p/L = 100$, our simulations show a sharp velocity selection near 0.7. This corresponds to a predominance of trajectories in which the polymer becomes trapped in a ring near the part of the cell where the external flow is of this magnitude, and will be further elucidated in the mass distribution results in Sec. III C. For $\ell_p/L = 10$, this peak persists but the distribution is more spread-out towards lower velocities, i.e., the polymer now preferentially becomes trapped

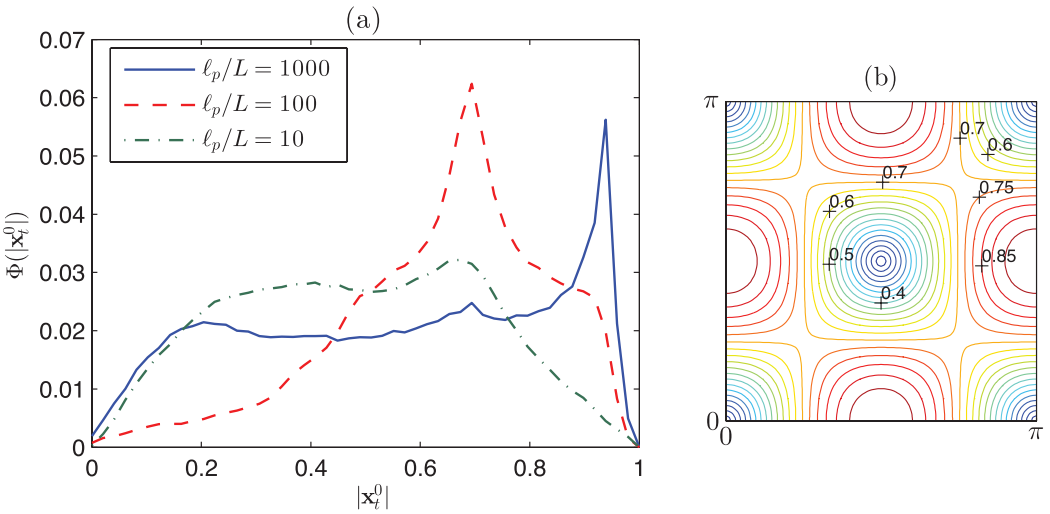

FIG. 4. (a) Frequency distribution of the magnitude of the center-of-mass velocity $|\mathbf{x}_t^0|$ for various values of ℓ_p/L at $\bar{\mu} = 20\,000$. (b) Contours of the fluid velocity magnitude inside a given cell, indicating that the value of $|\mathbf{x}_t^0| = 0.7$ corresponds approximately to the largest ring of uniform velocity within the cell.

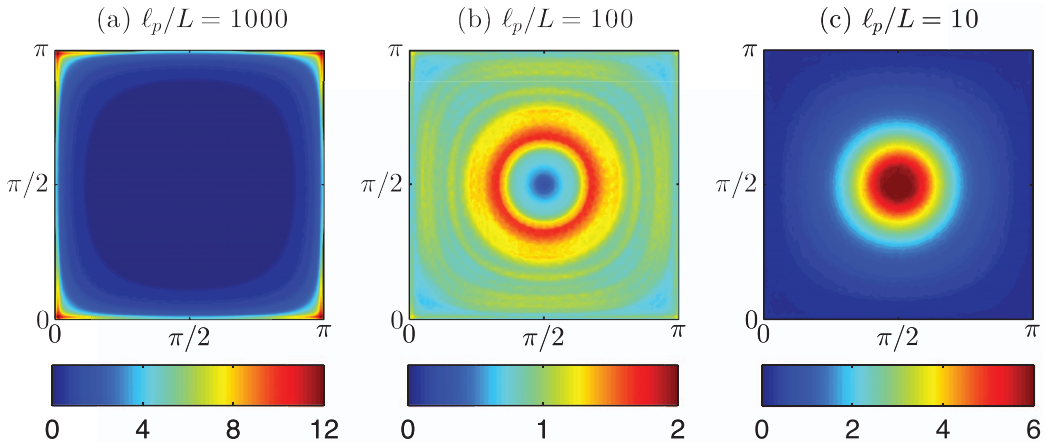

FIG. 5. Probability distributions of mass of the polymer in a unit cell at $\bar{\mu} = 20\,000$ for different values of ℓ_p/L. Probabilities are normalized to be unity for a uniform distribution.

in positions ranging all the way from the center of the cell to the ring of maximum uniform velocity.

C. Mass distribution of polymers

The preferred position of polymers inside the unit cell can be analyzed by considering the probability distributions of the mass of the entire polymer (which is assumed to be homogeneous along its backbone). Fig. 5 shows such distributions averaged over at least 50 simulations for three values of ℓ_p/L at $\bar{\mu} = 20\,000$. The plots are averaged across all cells that a polymer happens to be in, and are normalized to be unity for a uniform distribution.

The distribution for $\ell_p/L = 1000$ is unsurprising, as we recollect that this case is almost identical to the non-Brownian simulations[16] and the polymer is found to spend almost all of its time along the cell boundaries. Here again, the probability peaks near the corners, which reflects the slowing-down of the chain and time spent during buckling events around stagnation points (see Fig. 1). The floppier case of $\ell_p/L = 100$ looks qualitatively different and shows a characteristic ring of probability at a distance from the cell boundary. Here, we recall from the velocity distributions (Sec. III B) that the preferred center-of-mass velocity of a trapped polymer in this case is about 0.7. The ring that the center-of-mass must be on for this to happen is to the immediate outside of the concentration peak seen in Fig. 5(b). This shift inward is due to the cases when the polymer is aligned radially, thereby increasing the probability of finding a part of the chain in a circle of smaller radius. It is quite remarkable, however, that the polymer very rarely goes deeper into the cell beyond this ring, as shown by the low probability near the center. The floppiest case of $\ell_p/L = 10$ is qualitatively different from both previous cases. Here, the polymer selects velocities that place it closer to the center (Sec. III B) and the mass distribution indeed peaks there. Polymer centers-of-mass still move in rings around the center of the cell, but the aforementioned effect of radial alignment causes the peak to be at the center of the cell in this case. It should be noted when considering the distributions of Fig. 5 that they represent averages over a finite period of time and that their shape might change slightly if the simulations were run longer; also, they were obtained for polymers released along one of the cell edges and would likely show a stronger probability near the cell center for filaments released at arbitrary locations.

D. Cellular transport of rigid rods: A continuum approach

We have thus far demonstrated that flexibility affects transport properties in two distinct ways: on the one hand, it allows the filaments to buckle at the hyperbolic points, which facilitates their transport

across the lattice; on the other hand, it can also increase the importance of thermal fluctuations (by decreasing the persistence length), which has the opposite effect of driving polymers towards cell centers where they can become trapped. To further elucidate the effect of polymer flexibility in this transport process, we also approach the complementary problem of rigid Brownian rods from a continuum perspective. We do so by solving a conservation equation for the probability distribution function $\Psi(\mathbf{x}_0, \hat{\mathbf{p}}, t)$ of a single rod in a cellular flow, where the configuration of the rod is now described by its center-of-mass position $\mathbf{x}_0$ and a unit orientation vector $\hat{\mathbf{p}}$. Neglecting hydrodynamic interactions and limiting ourselves to two spatial dimensions (so that the rod orientation in the plane of the flow can be described by a single angle θ), we write down a Fokker-Planck equation[33] for the configuration of a particle as

$$\frac{\partial \Psi}{\partial t} + \nabla_x \cdot (\dot{\mathbf{x}}_0 \Psi) + \frac{\partial (\dot{\theta} \Psi)}{\partial \theta} - \nabla_x \cdot (\mathbf{D} \cdot \nabla_x \Psi) - d_r \frac{\partial^2 \Psi}{\partial \theta^2} = 0, \tag{11}$$

where $\mathbf{D}$ and d_r denote the translational and rotational diffusivities, respectively, and dots are meant to represent time derivatives. This conservation equation merely balances the time rate of change of the probability distribution Ψ with advection due to the effect of the external flow, and diffusion due to thermal fluctuations.

For a slender Brownian rod-like particle of length L and cross-sectional radius b, the rotational diffusivity d_r can be expressed as[33] $d_r = 3k_BT\ln(1/\epsilon)/\pi\mu L^3$ where we use the same definition of the aspect ratio $\epsilon = b/L$ as in Sec. II. The translational diffusivity tensor $\mathbf{D}$ is a sum of the contributions from the direction along the orientation of the rod, and that perpendicular to it. Given the translational diffusion coefficients[33] $D_\parallel = k_BT\ln(1/\epsilon)/2\pi\mu L$ and $D_\perp = k_BT\ln(1/\epsilon)/4\pi\mu L$ for motions in directions parallel and perpendicular to the rod axis, respectively, we express the diffusivity tensor as $\mathbf{D} = D_\parallel \hat{\mathbf{p}}\hat{\mathbf{p}} + D_\perp(\mathbf{I} - \hat{\mathbf{p}}\hat{\mathbf{p}})$, which simplifies to

$$\mathbf{D} = \frac{k_BT\,\ln(1/\epsilon)}{4\pi\mu L}(\mathbf{I} + \hat{\mathbf{p}}\hat{\mathbf{p}}). \tag{12}$$

Noting that this tensor only depends on the orientation of the rod and not on its position, and by virtue of its symmetry, we may write: $\nabla_x \cdot (\mathbf{D} \cdot \nabla_x \Psi) = \mathbf{D} : \nabla_x \nabla_x \Psi$.

The Fokker-Planck equation (11) requires knowledge of the translational and rotational fluxes, and these are evaluated based on slender-body theory in the Appendix. The final form of the conservation equation is then

$$\frac{\partial \Psi}{\partial t} + \mathrm{Pe}\left[\nabla_x \cdot \left\{\Psi \int_{-1/2}^{1/2} \mathbf{u}(\mathbf{x} + s\mathbf{p})\mathrm{d}s\right\} + \frac{\partial}{\partial \theta}\left\{12\Psi \hat{\mathbf{e}}_\theta \cdot (\mathbf{I} - \hat{\mathbf{p}}\hat{\mathbf{p}}) \cdot \int_{-1/2}^{1/2} s\mathbf{u}(\mathbf{x} + s\mathbf{p})\mathrm{d}s\right\}\right]$$
$$+ \ln\epsilon^2\left[\nabla_x^2\Psi + \hat{\mathbf{p}}\hat{\mathbf{p}} : \nabla_x\nabla_x\Psi + 12\frac{\partial^2\Psi}{\partial\theta^2}\right] = 0, \tag{13}$$

where we have introduced a Péclet number capturing the relative importance of advection by the flow to thermal diffusion:

$$\mathrm{Pe} = \frac{8\pi\mu\dot{\gamma}L^3}{k_BT} = \bar{\mu}\frac{\ell_p}{L}. \tag{14}$$

We note that this Péclet number also formally corresponds to the product of the dimensionless viscosity $\bar{\mu}$ and reduced persistence length ℓ_p/L, though neither quantity is defined on its own in the case of a rigid rod ($\bar{\mu} \to 0$ and $\ell_p/L \to \infty$). To determine the steady probability distribution function $\Psi(\mathbf{x}_0, \hat{\mathbf{p}})$, we integrate the conservation equation (13) by time-marching using an Adams-Bashforth scheme until it converges to a steady state. The imposed velocity $\mathbf{u}$ is of the same form as in Eq. (10), the aspect ratio is again set to $\epsilon = 0.01$, and the problem is solved on a four-cell unit ($W = \pi L$ here) of $\{x, y\} \in [-\pi, \pi]^2$ with periodic boundary conditions.

From the discussion of the buckling instability, we expect that polymers with rigid backbones (alternately interpreted as $\bar{\mu} < \bar{\mu}_c$) should not migrate past the cell they are initially placed in, a prediction indeed borne out by the experiments of Wandersman *et al.*[24] The numerical solution to the Fokker-Planck equation (13) corroborates this observation, as is seen in the steady probability contours of Fig. 6: for all values of Pe we considered, the probability peaks at the center of the cell

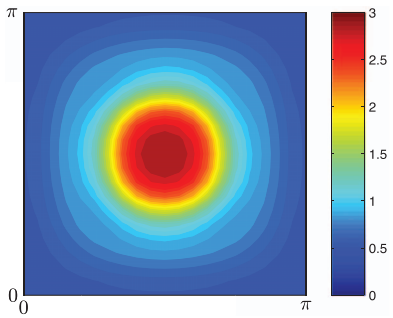

FIG. 6. Steady-state solution of the Fokker-Planck equation (13) at Pe = 10 000 for rigid rods of aspect ratio $\epsilon = 0.01$.

at steady state, with negligible presence near the cell boundaries. Unsurprisingly, this migration is found to become stronger with increasing Péclet number.

This case of rigid rods, characterized by a systematic drift towards and trapping near the center of the cells as seen in Fig. 6, can be contrasted to the case of elastic filaments to highlight the importance of filament flexibility in this transport process. Indeed, recalling that the Péclet number as defined here can be formally written as a product of the effective viscosity with the dimensionless persistence length, we compare distributions of filament configurations in two distinct simulations of semiflexible polymers at the same value of Pe but with different appropriately chosen values of $\bar{\mu}$ and ℓ_p/L (i.e., with different values of the bending resistance). We first set these parameters to $\bar{\mu} = 1000$ and $\ell_p/L = 1000$ (corresponding to Pe $= 10^6$) and show a superposition of representative filament configurations in Fig. 7(a). At this value of $\bar{\mu}$, the flow is not strong enough to induce buckling, and we indeed observe that the filament, which is hardly deformed by the flow, spends most of its time near the center of the cell, which follows from the prediction of the rigid rod theory in Fig. 6. However, the distribution of filament configurations looks qualitatively different in Fig. 7(b), where we choose parameter values of $\bar{\mu} = 10\,000$ and $\ell_p/L = 100$ (the product of which is the same as in the previous case) that do allow buckling. Here, the dynamics are found to differ from the predictions of the rigid rod theory, and a significant probability of finding the filament near the cell boundaries is clearly seen. As expected, we observe larger filament deformations, and fully buckled configurations are also seen near the corners of the cell. This increased probability of presence near the cell boundaries leads to more probable jumps across cells, which in turn results in more efficient transport across the cellular lattice as discussed previously.

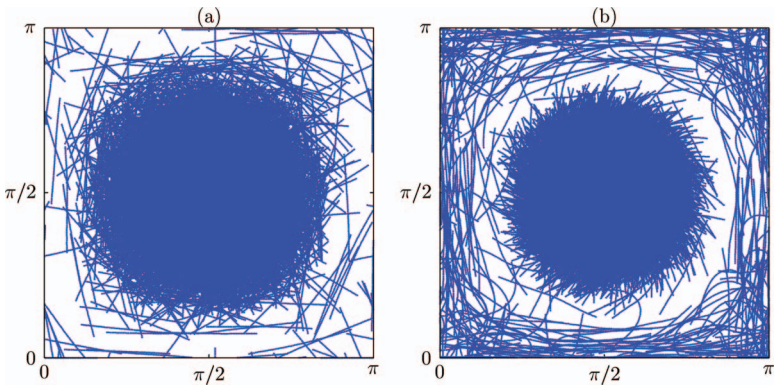

FIG. 7. Characteristic distributions of filament configurations in a unit cell with (a) $\bar{\mu} = 1000$ and $\ell_p/L = 1000$ and (b) $\bar{\mu} = 10\,000$ and $\ell_p/L = 100$.

IV. CONCLUDING REMARKS

We have used numerical simulations based on a slender-body model to study the dynamics and transport properties of semiflexible polymers in a periodic two-dimensional cellular flow in the presence of thermal fluctuations. This work extends previous theoretical[16] and experimental[24,25] studies that considered macroscopic non-Brownian filaments, and may also provide insight into some of the dynamics previously reported in actin motility assays.[20,21] As in the non-Brownian case, the strong compressive flows that occur near the hyperbolic stagnation points at the cell junctions can cause buckling of the filaments, which facilitates their transport between cells resulting in an effective two-dimensional random walk. However, we find that thermal fluctuations, quantified by the inverse of the dimensionless persistence length, tend to cause the filaments to drift towards and become trapped inside vortical cells for long periods of time. These frequent trapping events significantly hinder the spatial transport of the polymers, which shifts from diffusive to subdiffusive as fluctuations become significant, and this change in behavior is also evinced by the velocity and mass distributions of the chains. By comparing our simulation results to a simple theory for rigid Brownian rods, we also highlighted the subtle effect of flexibility on the transport properties. On the one hand, some level of flexibility is critical for the effective transport across cells as it enables buckling; on the other hand, very floppy filaments with short persistence lengths are strongly affected by thermal fluctuations, which cause their frequent trapping and hinder their transport across the lattice.

The model flow field considered in this work (periodic lattice of steady Taylor-Green vortices), through its simplicity, allowed us to arrive at a simple qualitative description of the dynamics in terms of transport and buckling along strain-dominated directions vs drifting and trapping inside vortical regions. It remains to be seen how this description would carry over to more complex flows, and in particular to unsteady chaotic flows with a spectrum of length scales such as a turbulent flow. While we expect the basic features of the dynamics observed here to also arise in that case, the net effect of flexibility and of thermal fluctuations on macroscopic rheological and transport properties[34,35] in complex flow fields remains difficult to anticipate.

ACKNOWLEDGMENTS

We thank Anke Lindner, Olivia du Roure, Nawal Quennouz, Raymond E. Goldstein, and Michael J. Shelley for enlightening discussions on various aspects of this work. We also gratefully acknowledge funding from NSF CAREER Grant CBET-1150590, from an FMC Educational Fund Fellowship, and from the University of Illinois Campus Research Board.

APPENDIX: FLUX VELOCITIES FOR THE FOKKER-PLANCK EQUATION

The conservation equation (11) has as unknowns the flux velocities of the rod. For this, we turn to the leading terms in the slender-body equation (1), now written in terms of the center-of-mass position and orientation of the particle. For a rod of aspect ratio $\epsilon = b/L$ as before and parameterized by $s \in [-L/2, L/2]$, the position of a point along the rod is now written as $\mathbf{x}_0 + s\hat{\mathbf{p}}$. We then have to leading order in $\ln\epsilon$,

$$\dot{\mathbf{x}}_0 + s\dot{\hat{\mathbf{p}}} - \mathbf{u}_0(\mathbf{x}_0 + s\hat{\mathbf{p}}) = \frac{\ln\epsilon}{4\pi\mu}(\mathbf{I} + \hat{\mathbf{p}}\hat{\mathbf{p}}) \cdot \mathbf{f}(\mathbf{x}_0 + s\hat{\mathbf{p}}). \tag{A1}$$

Integrating Eq. (A1) across the length of the rod and requiring that the total hydrodynamic force acting on the particle be zero gives the translational flux velocity:

$$\dot{\mathbf{x}}_0 = \frac{1}{L}\int_{-L/2}^{L/2} \mathbf{u}(\mathbf{x}_0 + s\hat{\mathbf{p}})\mathrm{d}s. \tag{A2}$$

In order to determine $\dot{\theta}$, we multiply Eq. (A1) by s and then integrate with respect to s giving

$$\dot{\hat{\mathbf{p}}}\frac{L^3}{12} - \int_{-L/2}^{L/2} s\mathbf{u}(\mathbf{x}_0 + s\hat{\mathbf{p}})\mathrm{d}s = \frac{\ln\epsilon}{4\pi\mu}(\mathbf{I} + \hat{\mathbf{p}}\hat{\mathbf{p}}) \cdot \int_{-L/2}^{L/2} s\mathbf{f}(\mathbf{x}_0 + s\hat{\mathbf{p}})\mathrm{d}s. \tag{A3}$$

Since the angular flux is purely in the orthoradial directions, we pre-multiply Eq. (A3) with $(\mathbf{I} - \hat{\mathbf{p}}\hat{\mathbf{p}})$, and it follows that

$$\dot{\hat{\mathbf{p}}}\frac{L^3}{12} = (\mathbf{I} - \hat{\mathbf{p}}\hat{\mathbf{p}}) \cdot \int_{-L/2}^{L/2} s\mathbf{u}(\mathbf{x}_0 + s\hat{\mathbf{p}})\mathrm{d}s - \frac{\ln\epsilon}{4\pi\mu}\hat{\mathbf{p}} \times \int_{-L/2}^{L/2} \hat{\mathbf{p}} \times s\mathbf{f}(\mathbf{x}_0 + s\hat{\mathbf{p}})\mathrm{d}s. \tag{A4}$$

Noting that the last term in Eq. (A4) represents the net torque acting on the particle, which is zero for a freely suspended particle, we obtain the final form of $\dot{\hat{\mathbf{p}}}$:

$$\dot{\hat{\mathbf{p}}} = \frac{12}{L^3}(\mathbf{I} - \hat{\mathbf{p}}\hat{\mathbf{p}}) \cdot \int_{-L/2}^{L/2} s\mathbf{u}(\mathbf{x}_0 + s\hat{\mathbf{p}})\mathrm{d}s. \tag{A5}$$

The angular velocity as required in Eq. (11) is then obtained as $\dot{\theta} = \dot{\hat{\mathbf{p}}} \cdot \hat{\mathbf{e}}_\theta$, where $\hat{\mathbf{e}}_\theta = (-\sin\theta, \cos\theta)$.

The Fokker-Planck equation is now closed, with all terms known. We non-dimensionalize Eq. (11) using characteristic scales of L for length, $8\pi\mu L^3/k_BT$ for time, and $L\dot{\gamma}$ for background velocities, yielding

$$\frac{k_BT}{8\pi\mu L^3}\frac{\partial\Psi}{\partial t} + \dot{\gamma}\nabla_x \cdot (\dot{\mathbf{x}}\Psi) + \dot{\gamma}\frac{\partial(\dot{\theta}\Psi)}{\partial\theta} - \frac{k_BT\ln(1/\epsilon)}{4\pi\mu L^3}(\mathbf{I}+\hat{\mathbf{p}}\hat{\mathbf{p}}) : \nabla_x\nabla_x\Psi - \frac{3k_BT\ln(1/\epsilon)}{\pi\mu^3}\frac{\partial^2\Psi}{\partial\theta^2} = 0. \tag{A6}$$

The coefficients are collected in the form of the Péclet number as defined in Eq. (14), and using Eqs. (A2) and (A5) for the flux velocities, we arrive at the final form given in Eq. (13).

[1] E. Lauga and T. R. Powers, "The hydrodynamics of swimming microorganisms," Rep. Prog. Phys. **72**, 096601 (2009).
[2] H. C. Ho and S. S. Suarez, "Hyperactivation of mammalian spermatozoa: function and regulation," Reproduction **122**, 519–526 (2001).
[3] T. Shinar, M. Mano, F. Piano, and M. J. Shelley, "A model of cytoplasmically-driven microtubule-based motion in the single-celled *C. elegans* embryo," Proc. Natl. Acad. Sci. U.S.A. **108**, 10508–10513 (2011).
[4] E. S. G. Shaqfeh, "The dynamics of single-molecule DNA in flow," J. Non-Newtonian Fluid Mech. **130**, 1–28 (2005).
[5] M. D. Graham, "Fluid dynamics of dissolved polymer molecules in confined geometries," Annu. Rev. Fluid Mech. **43**, 273–298 (2011).
[6] P. G. de Gennes, "Coil-stretch transition of dilute flexible polymers under ultrahigh velocity gradients," J. Chem. Phys. **60**, 5030–5042 (1974).
[7] C. M. Schroeder, H. P. Babcock, E. S. G. Shaqfeh, and S. Chu, "Observation of polymer conformation hysteresis in extensional flow," Science **301**, 1515–1519 (2003).
[8] C. Hsieh, L. Li, and R. Larson, "Modeling hydrodynamic interaction in Brownian dynamics: Simulations of extensional flows of dilute solutions of DNA and polystyrene," J. Non-Newtonian Fluid Mech. **113**, 147–191 (2003).
[9] R. G. Larson, *The Structure and Rheology of Complex Fluids* (Oxford University Press, New York, 1999).
[10] E. S. G. Shaqfeh, "Purely elastic instabilities in viscometric flows," Annu. Rev. Fluid Mech. **28**, 129–185 (1996).
[11] P. E. Arratia, C. C. Thomas, J. Diorio, and J. P. Gollub, "Elastic instabilities of polymer solutions in cross-channel flow," Phys. Rev. Lett. **96**, 144502 (2006).
[12] A. Groisman and V. Steinberg, "Elastic turbulence in a polymer solution flow," Nature **405**, 53–55 (2000).
[13] L. E. Becker and M. J. Shelley, "Instability of elastic filaments in shear flow yields first-normal-stress differences," Phys. Rev. Lett. **87**, 198301 (2001).
[14] A.-K. Tornberg and M. J. Shelley, "Simulating the dynamics and interactions of flexible fibers in Stokes flows," J. Comput. Phys. **196**, 8–40 (2004).
[15] G. K. Batchelor, "Slender-body theory for particles of arbitrary cross-section in Stokes flow," J. Fluid Mech. **44**, 419–440 (1970).
[16] Y.-N. Young and M. J. Shelley, "Stretch-coil transition and transport of fibers in cellular flows," Phys. Rev. Lett. **99**, 058303 (2007).
[17] L. Guglielmini, A. Kushwaha, E. S. G. Shaqfeh, and H. A. Stone, "Buckling transitions of an elastic filament in a viscous stagnation point flow," Phys. Fluids **24**, 123601 (2012).
[18] V. Kantsler and R. E. Goldstein, "Fluctuations, dynamics, and the stretch-coil transition of single actin filaments in extensional flows," Phys. Rev. Lett. **108**, 038103 (2012).
[19] K. Baczynski, R. Lipowsky, and J. Kierfeld, "Stretching of buckled filaments by thermal fluctuations," Phys. Rev. E **76**, 061914 (2007).
[20] L. Bourdieu, T. Duke, M. B. Elowitz, D. A. Winkelmann, S. Leibler, and A. Libchaber, "Spiral defects in motility assays: A measure of motor protein force," Phys. Rev. Lett. **75**, 176–179 (1995).
[21] L. Bourdieu, M. O. Magnasco, D. A. Winkelmann, and A. Libchaber, "Actin filaments on myosin beds: The velocity distribution," Phys. Rev. E **52**, 6573–6579 (1995).
[22] V. Schaller, C. Weber, C. Semmrich, E. Frey, and A. R. Bausch, "Polar patterns of driven filaments," Nature **467**, 73–77 (2010).
[23] T. Sanchez, D. Chen, S. DeCamp, M. Heymann, and Z. Dogic, "Spontaneous motion in hierarchically assembled active matter," Nature **491**, 431–434 (2012).

[24] E. Wandersman, N. Quennouz, M. Fermigier, A. Lindner, and O. du Roure, "Buckled in translation," Soft Matter **6**, 5715–5719 (2010).
[25] N. Quennouz, "Déformation et transport d'un filament élastique dans un écoulement cellulaire visqueux," Ph.D. thesis, Université Paris IV, 2013.
[26] T. Munk, O. Hallatschek, C. H. Wiggins, and E. Frey, "Dynamics of semiflexible polymers in a flow field," Phys. Rev. E **74**, 041911 (2006).
[27] F. Gittes, B. Mickey, J. Nettleton, and J. Howard, "Flexural rigidity of microtubules and actin filaments measured from thermal fluctuations in shape," J. Cell Biol. **120**, 923–934 (1993).
[28] M. F. Shlesinger, J. Klafter, and G. Zumofen, "Above, below and beyond Brownian motion," Am. J. Phys. **67**(12), 1253–1259 (1999).
[29] A. M. Lacasta, J. M. Sancho, A. H. Romero, I. M. Sokolov, and K. Lindenberg, "From subdiffusion to superdiffusion of particles on solid surfaces," Phys. Rev. E **70**, 051104 (2004).
[30] J.-P. Bouchaud and A. Georges, "Anomalous diffusion in disordered media: Statistical mechanisms, models and physical applications," Phys. Rep. **195**, 127–293 (1990).
[31] Q. Xu, L. Feng, R. Sha, N. C. Seeman, and P. M. Chaikin, "Subdiffusion of a sticky particle on a surface," Phys. Rev. Lett. **106**, 228102 (2011).
[32] J. S. Park and D. Saintillan, "From diffusive motion to local aggregation: Effect of surface contamination in dipolophoresis," Soft Matter **7**, 10720 (2011).
[33] M. Doi and S. F. Edwards, *The Theory of Polymer Dynamics* (Oxford University Press, Oxford, 1986).
[34] V. E. Terrapon, Y. Dubief, P. Moin, E. S. G. Shaqfeh, and S. K. Lele, "Simulated polymer stretch in a turbulent flow using Brownian dynamics," J. Fluid Mech. **504**, 61–71 (2004).
[35] J. S. Paschkewitz, Y. Dubief, and E. S. G. Shaqfeh, "The dynamic mechanism for turbulent drag reduction using rigid fibers based on Lagrangian conditional statistics," Phys. Fluids **17**, 063102 (2005).